A Ripple Reduction Method for a Two Stages Battery Charger with Multi-winding Transformer using Notch Filter

Haimeng Wu*,Volker Pickert*, Simon Lambert*, Peter Allan†, Xu Deng*, Huaxia Zhan*
*School of Electrical and Electronic Engineering,Newcastle University,Newcastle upon Tyne,UK.
†Hyperdrive innovation LTD, Gateshead, Newcastle upon Tyne, UK
Haimeng.wu@ncl.ac.uk

***Abstract*-This paper presents a two-stage battery charger consisting of a bridgeless Totem-pole power factor correction (TP-PFC) circuit and a full bridge converter with a multi-winding transformer. By using this transformer the cell equalizing operation can be achieved with no additional circuitry. In addition, a double-line frequency ripple reduction method is proposed to address the low frequency current ripples issues existing in both primary and secondary winding of the transformer which is caused by the voltage ripples across the intermediate DC link bus. Control and analysis of the converter at different operation modes is illustrated in detail and simulation results validate the effectiveness of the proposed converter and control algorithm.**

I. INTRODUCTION

Battery charger technologies have been developed over the years to improve the performance of system and reduce the cost of equipment, meeting the demand in the various energy storage system, such as hybrid electric vehicle (HEV) and renewable energy generation system [1-3]. The converters used in most of such applications can be generally classified into single-stage and two-stage class. Single-stage converters have fewer components offering a low cost solution but comes with the limitations of generating large amount of low frequency ripple across batteries which is mainly twice of the line frequency [4]. In contrast, two stage chargers have the inherent feature of rejecting low frequency ripples [3]. And most two-stage converters require large capacitors that are normally designed to cope with the high voltage ripple across the DC bus link which results in size, weight and cost gains. However, for the cost-driven applications of applying capacitors with reduced capacitance, higher rated components must be employed to cope with ripples. Consequently, higher losses can be produced which leads to the decrease of the overall efficiency of the converter.

Front-end AC-DC converter is a key component for any battery charger system and power factor correction (PFC) is required when connected to the AC power grid. The evaluation and efficiency comparison of various types of AC-DC PFC converter has been presented in [5], where the bridgeless PFC converter shows a remarkable performance in terms of power conversion efficiency. For the DC-DC converters after PFC circuit, there are many candidate topologies presented as EV battery charger charging battery packs which consist of a string of individual battery cells [6, 7] . However, it is well known that battery cells have voltage mismatch between them mainly due to manufacturing tolerances. To ensure safe and reliable operation of battery packs a battery management system must be required that equalizes each cell using various types of equalisation circuits [8-12] . Passive and active battery balancing techniques comparison has been compared in [13] concluding that active balancing circuits increase cost and complexity of the system.

Although the double-line-frequency ripple component is relatively small in two stage battery charger compared with single stage counterparts, it can bring in issues of increased current ripple especially when small DC link capacitor employed. Some papers have discussed the solutions of reducing the ripples in photovoltaic (PV) two-stage inverter application using DC-link voltage feed-forward method [14] or through an additional circuit using a front-end buck-type dc/dc converter [15], but not in the two-stage AC-DC single phase converters where the issue of double-line-frequency ripple cannot be neglected.

In this paper, a two stages battery charger with a multi-winding transformer is proposed using the bridgeless Totem-pole power factor correction (TP-PFC) circuit as the front-end AC-DC converter. This battery charger differs as such that it charges each cell without the help of an active balancing circuit. This is due to the structure of multi-winding transformer and operation of the converter. In addition, to address the issue of the double line frequency current ripples in both the primary and secondary winding current, a ripple reduction method is proposed using a Notch filter. Simulation results show that this low frequency ripple can be significantly reduced which demonstrates the effectiveness of the proposed control algorithm.

II. PROPOSED TOPOLOGY AND OPERATION

A. Operation of TP-PFC

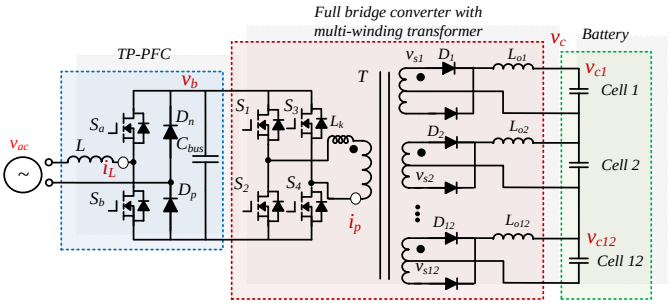

Fig. 1 Diagram of the proposed battery charger

The diagram of the proposed battery charger is shown in the Fig. 1, which is a two-stage AC-DC converter consisting of a bridgeless TP-PFC circuit and a full bridge converter with

the multi-winding transformer. This converter achieves battery cells charging and balancing without using additional circuitry. The TP-PFC circuit is chosen as the front-end converter since its high power conversion efficiency compared with the traditional PFC circuit. Specifically, there are only two components conducted in each subinterval of operation, in contrast, three components are conducted in traditional counterpart. The key waveforms and the control blocks of TP-PFC circuit are illustrated in Fig. 2(a) and Fig. 2(b) respectively.

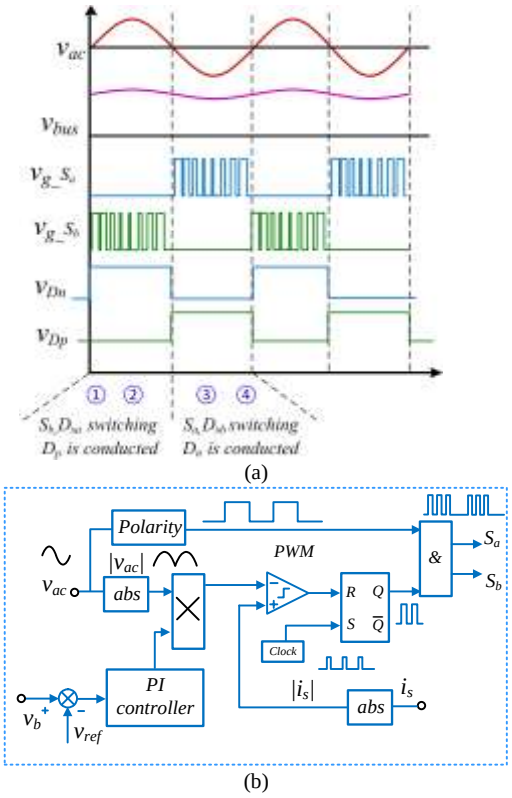

Fig. 2 (a) Diagram of the key waveforms of TP-PFC circuit (b) Corresponding control blocks

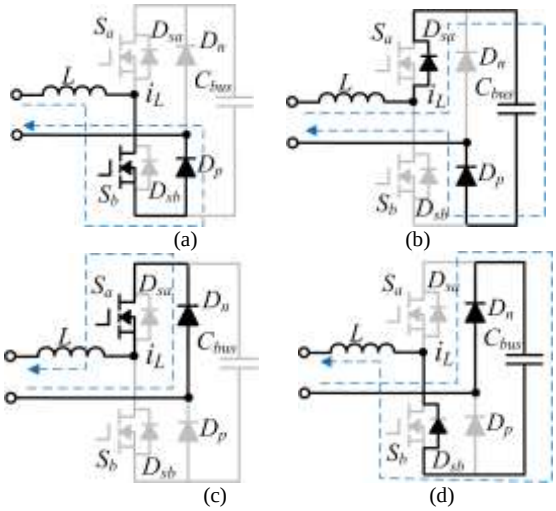

Fig. 3 subintervals of TP-PFC operation

Fig. 3 presents the corresponding subintervals of circuit operation. The switches S_a and S_b are operated at high switching frequency with their body diodes. While diodes D_p and D_n are conducted at line frequency when the AC grid is in the positive and negative half period respectively.

The intermediate DC link capacitor play a role as an energy buffer, and the relationship between required capacitance and ripple voltage for this single-phase AC–DC converter can be obtained as

$$C_{bus} > \frac{V_{ac} \cdot I_{ac}}{2\pi f_s \cdot \eta \cdot V_b^2} \quad (1)$$

where V_{ac} , I_{ac} are the RMS values of line voltage and current, respectively, f_s is the line frequency, η is the required peak to peak ripple percentage of the average value of the DC link voltage V_b.

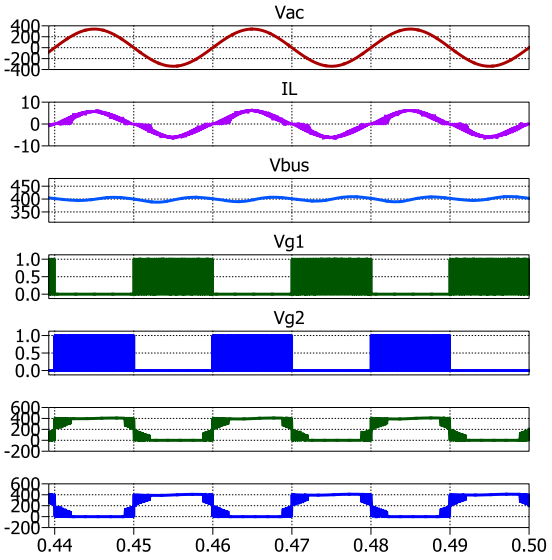

Fig.4 Simulation results of TP-PFC circuit

Fig.4 shows the simulation results of the TP-PFC circuit, which are the waveforms of the grid voltage v_{ac}, the current through inductor i_L, the voltage across the DC link capacitor v_b, the drives signals of switch S_a and S_b, and the voltages across diodes D_n and D_p.

Due to the DC link bus capacitor, the operational modes of the full bridge converter can be considered that they are free from frequency ripples caused by the switching action from the front-end circuit. The only significant remaining impact is the double line frequency voltage ripples across this DC capacitor.

B. Study on full bridge converter with muti-winding converter

The diagram of the key operational waveforms of the DC-DC converter after PFC circuit is presented in Fig.5. S_1 and S_4, S_2 and S_3 are conducted with the same PWM drive signal respectively, and there are 180 degree phase shift between them. It should be noted that because of the leakage inductance, there is a small period when the both the switches are turned off. The energy stored in the leakage inductor is released through the parasitic capacitors across the switches.

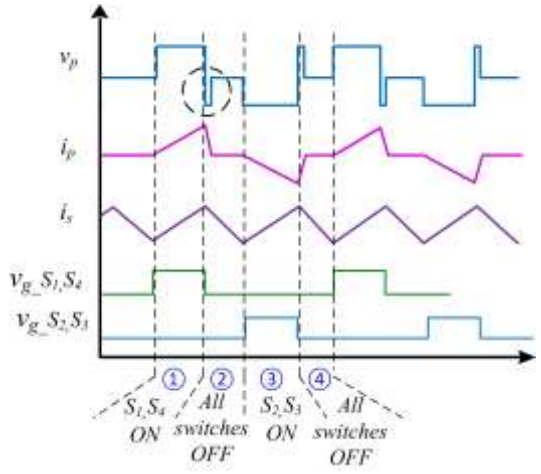

Fig.5 Diagram of the key operational waveforms of full bridge converter with muti-winding transformer

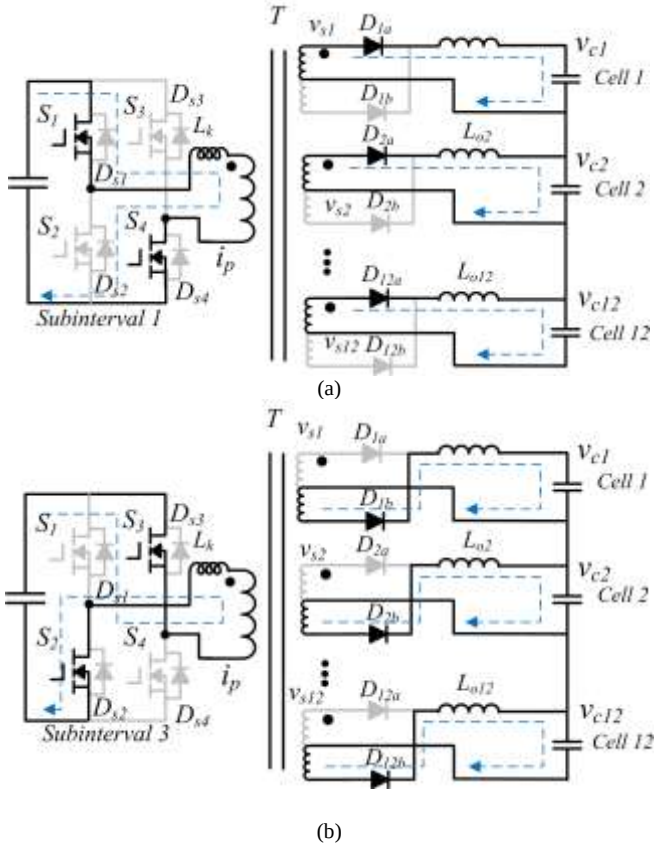

Fig.6 subinterval operation of the full bridge converter with multi-windings

Fig.6 illustrates the key subinterval operation of this full bridge converter with multi-windings. In the first subinterval, S_1, S_4 and D_{na} are conducted. The expressions of the primary voltage v_p, the secondary voltage v_{sn} across transformer, the current i_{sn} and the current ripples Δi_{sn} through output inductor L_{on} ($n=1,2\ldots12$) in the secondary can be obtained as follows:

$$v_p = V_b(1+\eta\cdot\cos(2\omega t)) \tag{2}$$

$$v_{sn} = \frac{1}{n}v_p \tag{3}$$

$$\Delta i_{sn} = \frac{(v_{sn}-v_{dn}-v_{cn})\cdot dT_s}{L} \tag{4}$$

$$i_{sn} = I_{sn} + \frac{\Delta i_{sn}}{2} \tag{5}$$

From equations (2)~(5), i_{sn} can be expressed as:

$$i_{sn} = I_{sn} + \frac{(V_b(1+\eta\cdot\cos(2\omega t))/n - v_{dn} - v_{cn})\cdot dT_s}{2L} \tag{6}$$

where ω is the line frequency in rad/s, n is the turn ratio, d represents the duty cycle, I_{sn} is the averaged value of the output current to cells, and v_{dn} an v_{cn} are the voltage drops on secondary diodes and the voltage on cells respectively. The voltage drops across the Mosfets are not considered in the expression because the values are relatively small to the DC link voltage.

In the second subinterval, the following equations can be obtained:

$$v_{sn} = \frac{1}{n}v_p = 0 \tag{7}$$

$$\Delta i_{sn} = \frac{-(v_{dn}+v_{cn})\cdot(0.5-d)T_s}{L} \tag{8}$$

$$i_{sn} = I_{sn} + \frac{-(v_{dn}+v_{cn})\cdot(0.5-d)T_s}{2L} \tag{9}$$

In the steady state, by applying the principle of volt-second balance to the output filter inductor L_{on}, the expression of duty cycle d is derived as:

$$d = \frac{0.5\cdot(v_{cn}-v_{dn})}{V_b(1+\eta\cdot\cos(2\omega t))/n - 2v_{dn}} \tag{10}$$

From equation (10), it is evident that the duty cycle cannot be constant for the steady state operation, which is related with the values of the voltage ripple and line frequency.

In the third subinterval, the S_1, S_4 and D_{nb} are conducted and the voltage and current stress are identical as the equation shown in (2)~(6).

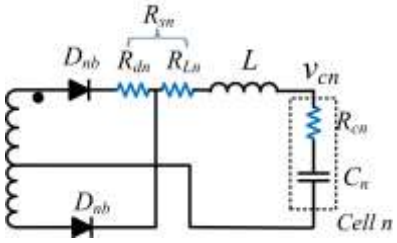

Fig.7 Diagram of secondary with parasitic parameters

From the equation (6), it can been seen that when the muti-winding transformer have identical turn ratio n, the battery cells with lower initial voltage will bear higher charging current, which thereby results in a natural cell balancing during the charging mode. As shown in Fig.7, the parasitic parameter such as ESRs of the secondary diodes (R_{dn}), the output inductor (R_{Ln}) and the battery cells (R_{cn}) must be considered in practical circuit as they are critical to the cells balancing performance during charging. Assuming that two cells have identical parasitic but the different initial voltage

v_{c1} and v_{c2}, the charging in the second subinterval becomes as follows:

$$i_{sn} = I_{sn} + \frac{-(i_{sn}R_{sn} + i_{sn}R_{cn}v_{dn} + v_{cn}) \cdot (0.5-d)T_s}{2L} \quad (11)$$

where R_{sn} is the sum of R_d and R_L, It can be represented in the following form:

$$i_{sn}(1+\frac{(R_{sn}+R_{cn})(0.5-d)T_s}{2L}) = I_{sn} + \frac{-(v_{dn}+v_{cn}) \cdot (0.5-d)T_s}{2L} \quad (12)$$

Assuming that parasitic parameters of each cell are identical, the difference between two charging current can be obtained:

$$\begin{aligned}&(i_{s1}-i_{s2})(1+\frac{(R_s+R_c)(0.5-d)T_s}{2L}) \\ &= (I_{s1}-I_{s1}) + \frac{(v_{c2}-v_{c1}) \cdot (0.5-d)T_s}{2L}\end{aligned} \quad (13)$$

In the steady state, the difference of instantaneous value of current is identical with the averaged one, thus

$$i_{s1} - i_{s2} = I_{s1} - I_{s1} \quad (14)$$

From (13) and (14), the following expression can be obtained:

$$i_{s1} - i_{s2} = \frac{v_{c2}-v_{c1}}{R_s+R_c} \quad (15)$$

This equation reveals that the EMS values of R_s and R_c determine the difference of charging current among the battery cells with different initial voltages.

III. Proposed Ripple Reduction Method Using Notch Filter

From equation (10), it can be see that for the ideal steady-state operation, the control signals of switches must contains the terms of the double line frequency in the denominator which is to ensure the suppression of the ripple influence from the DC link capacitor. However, in the conventional averaged constant current and constant voltage control strategy for battery charger, the PWM signals are generated either after an inner current loop (constant current mode) or outer voltage loop plus inner current loop (constant voltage mode). The ripple component will exist in the measured primary current and will reflect in the control signal. It is also noted that the phase shift φ can be produced if filters and compensators are employed in the control loop. Thus the expression of PWM duty cycle can be given as:

$$d = \frac{v_{con}}{V_m} = \frac{V_{con}(1+\cos(2\omega t+\varphi))}{V_m} \quad (16)$$

where V_m is the amplitude value of the sawtooth waveform and V_{con} is the averaged value of control signal. And this value of φ cannot be directly obtained without using complicated system modelling approaches. Thereby this controlled PWM signal causes a considerable double line frequency ripple component both in the secondary which results in the higher peak and RMS values of current. In order to supress this ripple influence, a ripple reduction method using Notch filter is proposed in this section.

Notch filter is a kind of band-stop filters with a narrow band width and high quality factor. The expression of Notch filter in the s domain is shown as follows:

$$H(s) = \frac{s^2+\omega_c^2}{s^2+2\xi\omega s+\omega_c^2} \quad (17)$$

Using a tuned Notch filter, a certain frequency of the signal can be eliminated to keep the rest effective components of this signal. Fig.8 shows the control algorithm of this converter that demonstrates the implementation of Notch filter in the control system. By tuning the target frequency ω_c (ω_c=50Hz), quality factor ξ(ξ=*1*) and Notch gain (k_n), the unexpected components in the control signal caused by the low frequency current ripple can be eliminated and a compensation signal from DC link bus can be generated to compensate the filtered control signal. The concept of this method is to extract the ripple component from v_b. After the operation of proportional, this ripple signal is injected to the original control signal v_{ctl} that is processed by the Notch filter, generating a final control signal v_{con}. After applying this proposed method, the expression of duty cycle has been changed as

$$d = \frac{v_{con}}{V_m} = \frac{V_{con}(1-\eta\cos(2\omega t))}{V_m} \quad (18)$$

When $\eta^2 << 1$, the outcome of equation (18) is close to equation (10) where the derived duty cycle is able to get rid of the influence of double line frequency ripple. To meet the demand of compensation, the required gain k_n shown in Fig.8 is given as follows:

$$k_n = V_{ctl} \cdot \eta \quad (19)$$

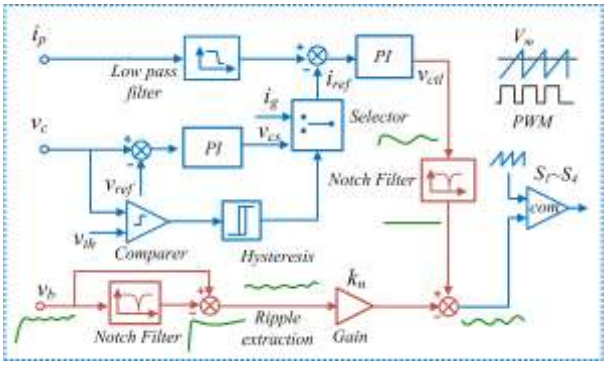

Fig.8 Control algorithm of full bridge based converter with the multi-winding transformer

IV. Simulation Verifications

The specification of simulation is presented in TABLE I, and the key operational waveforms of the full bridge converter with multi-winding are shown in Fig.9(a), including the input voltage, the current of TP-PFC circuit, the voltage across DC link capacitor, the voltage and current of primary winding and the current in the secondary. When 4 of 12 cells are set with different initial values: 3.60, 3.65, 3.70 and 3.80V, and rest cells are 3.75V, it can be seen that the difference among them are gradually decreased during the process of charging mode. Fig.9 (b) and Fig.9 (c) illustrate the waveforms of the voltage and current of the battery cells at cell balancing process respectively.

TABLE I
SPECIFICATION OF SIMULATION

Parameters	Value	Parameters	Value
Frequency(kHz)	**50**	Magnetizing inductance (μH)	**inf**
Output power (W)	**880**	Nominal output voltage of cells (V)	**3.75**
Capacitance of Cell (F)	**30**	ESR of cell (mΩ)	**1**
Inductance of Boost PFC (μH)	**500**	Capacitance of Boost PFC (μF)	**500**
Output inductance (μH)	**0.33**	Leakage inductance (μH)	**10**
Number of Primary turns	**60**	Number of Secondary turns	**1**
Voltage drop of secondary diodes	**0.3**	Number of cells	**12**

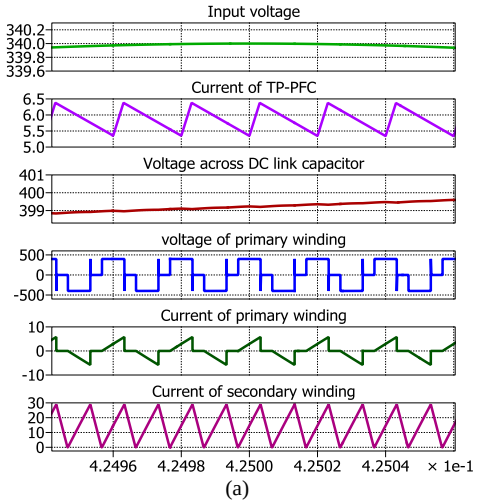

(a)

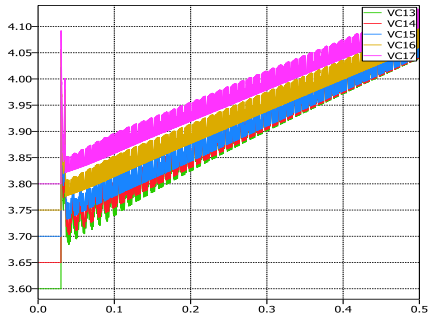

(b)

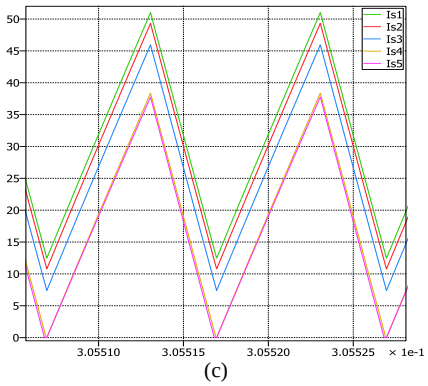

(c)

Fig.9 (a) Key operational waveforms of the full bridge converter with muti-windings (b), (c) Waveforms of battery cell voltage and current at cell balancing process with different initial voltages

Fig.10(a) shows the key signals in the control blocks which are measured DC link voltage signal v_b, the signal of v_b after Notch filer, the extraction ripple signal v_{rp} and the constructed control signal v_{con}. Fig.10(b) presents simulation results of the converter with and without employing the proposed ripple reduction methods. The switching of the control methods takes place at time of 0.4s, it can be seen that the peak to peak value of the primary and secondary at double line frequency has been reduced from 12.5% to less than 1%, which successfully demonstrate the effectiveness of the proposed control method. Therefore, using the proposed control algorithm, the ripple can be significantly reduced and both the peak and RMS values in the primary and secondary can be decreased to enhance the power conversion efficiency.

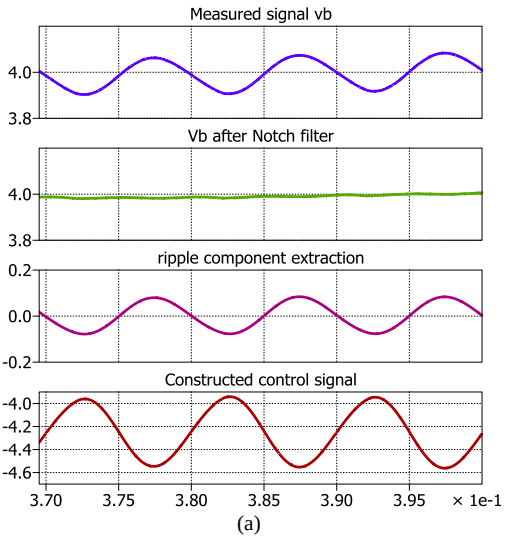

(a)

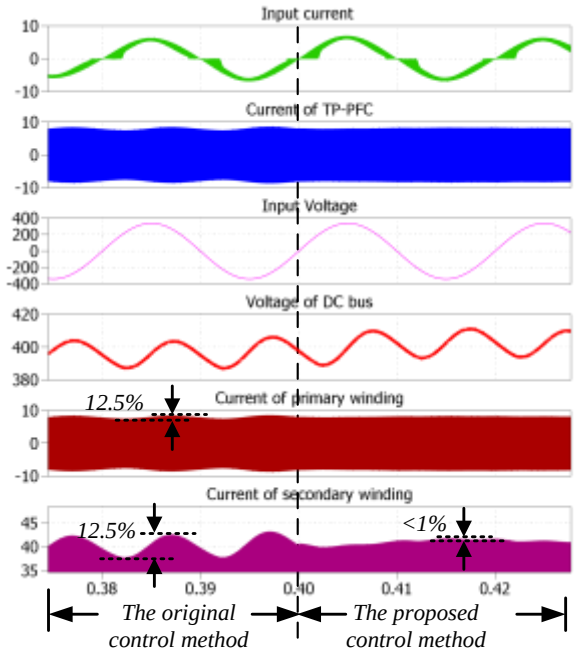

(b)

Fig.10 (a) key signals in the control blocks
(b) Comparison of the converter using original method and proposed method

V. CONLUSION

In conclusion, a two-stage battery charger with integrated cell balancing using the multi-winding transformer and a double-line frequency ripple reduction method is proposed in this paper. This converter integrates the battery charging with cell balancing where both operations are working simultaneously with no additional cells equaliser. Moreover, the proposed ripple cancellation approach has significantly reduced the low frequency current ripples in both sides of the transformer, which improves system performance.

ACKNOWLEDGMENT

The authors would like to acknowledge Innovate UK and Hyperdrive innovation LTD for the full sponsorship and support in this project.

REFERENCES

[1] Z. Liu, B. Li, F. C. Lee, and Q. Li, "Design of CRM AC/DC converter for very high-frequency high-density WBG-based 6.6kW bidirectional on-board battery charger," in *2016 IEEE Energy Conversion Congress and Exposition (ECCE)*, 2016, pp. 1-8.

[2] W. Li, H. Wu, H. Yu, and X. He, "Isolated Winding-Coupled Bidirectional ZVS Converter With PWM Plus Phase-Shift (PPS) Control Strategy," *IEEE Transactions on Power Electronics*, vol. 26, pp. 3560-3570, Dec 2011.

[3] F. Musavi, W. Eberle, and W. G. Dunford, "A High-Performance Single-Phase Bridgeless Interleaved PFC Converter for Plug-in Hybrid Electric Vehicle Battery Chargers," *IEEE Transactions on Industry Applications*, vol. 47, pp. 1833-1843, 2011.

[4] H. Vig and D. Bourner, "PFC Single Conversion Line Ripple Cancellation Using the Yeaman Topology," in *PCIM Europe 2014; International Exhibition and Conference for Power Electronics, Intelligent Motion, Renewable Energy and Energy Management*, 2014, pp. 1-8.

[5] F. Musavi, M. Edington, W. Eberle, and W. G. Dunford, "Evaluation and Efficiency Comparison of Front End AC-DC Plug-in Hybrid Charger Topologies," *IEEE Transactions on Smart Grid*, vol. 3, pp. 413-421, 2012.

[6] D. Gu, Z. Zhang, Y. Wu, D. Wang, H. Gui, and L. Wang, "High efficiency LLC DCX battery chargers with sinusoidal power decoupling control," in *2016 IEEE Energy Conversion Congress and Exposition (ECCE)*, 2016, pp. 1-7.

[7] L. Xue, Z. Shen, D. Boroyevich, P. Mattavelli, and D. Diaz, "Dual Active Bridge-Based Battery Charger for Plug-in Hybrid Electric Vehicle With Charging Current Containing Low Frequency Ripple," *IEEE Transactions on Power Electronics*, vol. 30, pp. 7299-7307, 2015.

[8] G. Oriti, A. L. Julian, and P. Norgaard, "Battery management system with cell equalizer for multi-cell battery packs," in *2014 IEEE Energy Conversion Congress and Exposition (ECCE)*, 2014, pp. 900-905.

[9] Z. Huaxia, X. Xin, S. M. Lambert, V. Pickert, W. Haimeng, and L. Xiang, "A cascaded transformer-based equalisation converter for series connected battery cells," in *8th IET International Conference on Power Electronics, Machines and Drives (PEMD 2016)*, 2016, pp. 1-6.

[10] N. Tashakor, E. Farjah, and T. Ghanbari, "A Bidirectional Battery Charger With Modular Integrated Charge Equalization Circuit," *IEEE Transactions on Power Electronics*, vol. 32, pp. 2133-2145, 2017.

[11] S. Lambert, V. Pickert, D. Atkinson, and H. Zhan, "Transformer-Based Equalization Circuit Applied to <italic>n</italic>-Number of High Capacitance Cells," *IEEE Transactions on Power Electronics*, vol. 31, pp. 1334-1343, 2016.

[12] S. Li, C. C. Mi, and M. Zhang, "A High-Efficiency Active Battery-Balancing Circuit Using Multiwinding Transformer," *IEEE Transactions on Industry Applications*, vol. 49, pp. 198-207, 2013.

[13] M. Daowd, N. Omar, P. V. D. Bossche, and J. V. Mierlo, "Passive and active battery balancing comparison based on MATLAB simulation," in *2011 IEEE Vehicle Power and Propulsion Conference*, 2011, pp. 1-7.

[14] J. Viinamäki, J. Jokipii, and T. Suntio, "Improving double-line-frequency voltage ripple rejection capability of DC/DC converter in grid connected two-stage PV inverter using DC-link voltage feedforward," in *2016 18th European Conference on Power Electronics and Applications (EPE'16 ECCE Europe)*, 2016, pp. 1-10.

[15] X. Zhao, L. Zhang, R. Born, and J. S. Lai, "Solution of input double-line frequency ripple rejection for high-efficiency high-power density string inverter in photovoltaic application," in *2016 IEEE Applied Power Electronics Conference and Exposition (APEC)*, 2016, pp. 1148-1154.